This is an open access article published under an ACS AuthorChoice License, which permits copying and redistribution of the article or any adaptations for non-commercial purposes.

NANO LETTERS

Letter

pubs.acs.org/NanoLett

Polarization-Dependent Optical Response in Anisotropic Nanoparticle–DNA Superlattices

Lin Sun,[†,‡] Haixin Lin,[‡,§] Daniel J. Park,[‡,§] Marc R. Bourgeois,[§] Michael B. Ross,[‡,§] Jessie C. Ku,[†,‡] George C. Schatz,*[,‡,§] and Chad A. Mirkin*[,†,‡,§]

[†]Department of Materials Science and Engineering, [‡]International Institute for Nanotechnology, and [§]Department of Chemistry, Northwestern University, Evanston, Illinois 60208 United States

Supporting Information

ABSTRACT: DNA-programmable assembly has been used to prepare superlattices composed of octahedral and spherical nanoparticles, respectively. These superlattices have the same body-centered cubic lattice symmetry and macroscopic rhombic dodecahedron crystal habit but tunable lattice parameters by virtue of the DNA length, allowing one to study and determine the effect of nanoscale structure and lattice parameter on the light-matter interactions in the superlattices. Backscattering measurements and finite-difference time-domain simulations have been used to characterize these two classes of superlattices. Superlattices composed of octahedral nanoparticles exhibit polarization-dependent backscattering but via a trend that is opposite to that observed in the polarization dependence for analogous superlattices composed of spherical nanoparticles. Electrodynamics simulations show that this polarization dependence is mainly due to the anisotropy of the nanoparticles and is observed only if the octahedral nanoparticles are well-aligned within the superlattices. Both plasmonic and photonic modes are identified in such structures, both of which can be tuned by controlling the size and shape of the nanoparticle building blocks, the lattice parameters, and the overall size of the three-dimensional superlattices (without changing habit).

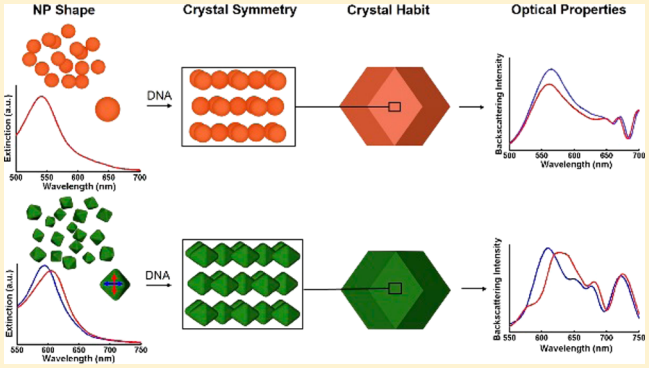

KEYWORDS: *DNA-programmable assembly, anisotropic nanoparticles, plasmonics, polarization*

Gold nanoparticles (NPs) are widely studied optical building blocks due to their strong interactions with visible light, which is confined into small volumes close to the NP surface due to localized surface plasmon resonance (LSPR) excitation.[1−6] The LSPR is sensitive to NP size, shape, composition, dielectric environment, and proximity to other plasmonic NPs.[7−10] Ordered arrays and other structures of plasmonic NPs exhibit a variety of interesting properties, such as the ability to guide light around sharp corners,[11] a broadband optical response,[12] Fano resonances,[13] and a negative index, which is important for the development of metamaterials.[14] Moreover, the optical properties of such ordered plasmonic structures can be tuned by changing the distance between individual NPs.[7−9,15,16] Therefore, great effort has been devoted to research on making two- and three-dimensional periodic structures of plasmonic NPs using top down[11,12,14] and bottom up[10,17−19] techniques.

DNA-programmable assembly has emerged as a robust and flexible tool for synthesizing superlattices with control over NP size and shape, lattice structure, and crystal habit. In these structures, nanoparticles with different shapes,[20,21] sizes,[22] and compositions[21,23,24] can be assembled and also lattice symmetry and nanoparticle spacing can be tuned,[22,25] giving rise to robust[26] and compositionally tunable thin film optical modes.[24] In addition, the micron length scales associated with well-formed superlattices lead to optical cavity modes, such as FP resonances[27] that arise due to interference of light traveling between the parallel top and bottom facets of the superlattice,[27,28] and shape-dependent scattering[29] that is dictated by the crystal habit (i.e., the size and shape of the micro- or macroscopic superlattice). In principle, one can uniquely use DNA-programmable methods to assemble different NP building blocks into macroscopic superlattices where the superlattices have the same crystal symmetry and macroscopic crystal habit but that comprise different NP shapes. This type of comparison enables separation of the effect of NP shape from the effects of lattice symmetry and microscale faceting.

Herein, we show that octahedral and spherical NPs can be assembled into body-centered cubic (bcc) superlattices with identical rhombic dodecahedra crystal habits and similar lattice parameters but different optical properties (Figure 1). These superlattices have been characterized by backscattering measurements and finite-difference time-domain (FDTD) simulations. In addition to focusing on the importance of the

Received: December 8, 2016
Revised: February 23, 2017
Published: March 30, 2017

Downloaded via OFFICE OF SCIENTIFIC AND TECHL INFO on September 27, 2018 at 12:32:00 (UTC).
See https://pubs.acs.org/sharingguidelines for options on how to legitimately share published articles.

 © 2017 American Chemical Society

DOI: 10.1021/acs.nanolett.6b05101
Nano Lett. 2017, 17, 2313−2318

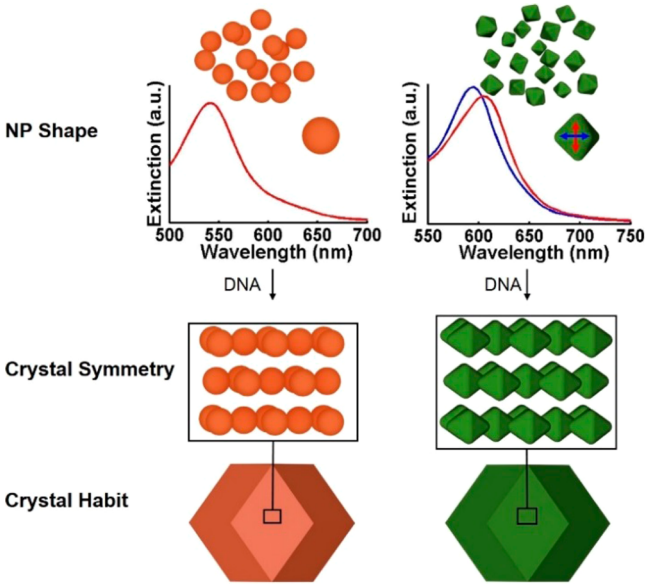

Figure 1. Schematic depiction of the structure of superlattices made from either spherical (orange) or octahedral (green) NPs. The shape of the NPs gives rise to different polarization dependence of their LSPRs. Both superlattices have bcc lattice structures and the exposed facets are the closest packed (110) planes for the rhombic dodecahedral crystal habit. Single nanoparticle extinction spectra were obtained from FDTD calculations with the refractive index of the dielectric environment set as 1.45. Note that different wavelength ranges are used in the spectra.

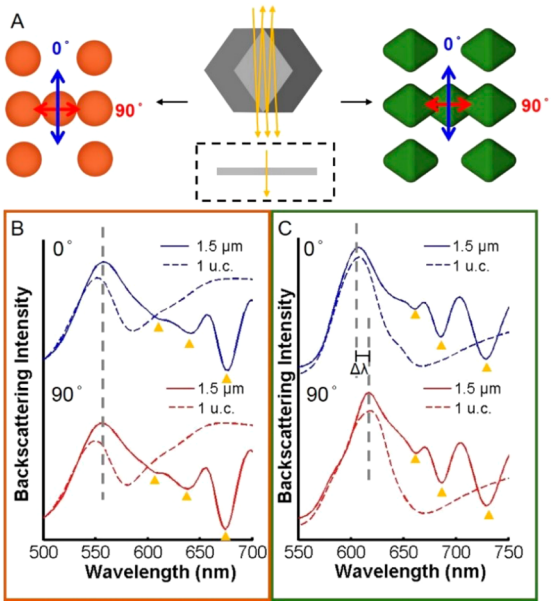

Figure 2. Optical modes of the superlattice consist of both plasmonic and FP modes. The roles of each mode are shown in the backscattering spectra. (A) Schematic depiction of the superlattice where both plasmonic and FP modes exist in comparison to a thin slab with a thickness of only 1 u.c., which is too thin to support FP modes (center). Structures of a single unit cell of superlattices made from spherical (left) and octahedral (right) NPs along the (110) direction are shown with the 0° and 90° indicating the corresponding polarizations of the incident light. (B) FDTD simulation of a spherical superlattice with the polarization along 0° (top, solid line) and 90° (bottom, solid line) as defined in (A). The gray dashed line indicates the maximum wavelength of the main peaks, which is the same for the two polarizations. The blue and red dashed lines are the spectra of the 1 u.c. thick slab, which shows that the location of the main peak is determined by the plasmonic modes. The dips at longer wavelength, as indicated by the yellow arrows, are FP modes. (C) The same simulations were performed for superlattices made from octahedral NPs, where there is a difference ($\Delta\lambda \sim 10$ nm) between the main peaks of the two polarizations.

shape of the NPs, we can also use simulations and, in certain cases, experiment to independently assess the importance of lattice parameter and size of the microscale superlattices on optical response. Therefore, this DNA-programmable technique allows one to separate contributions of the nanoscale building blocks from the microscale architecture to the optical properties of the superlattice. Importantly, superlattices composed of octahedral NPs exhibit polarization-dependent backscattering spectra at all volume fractions studied (5.1−20.3%), while the opposite polarization dependence behavior is seen in superlattices composed of spherical NPs with volume fractions larger than 10%. Finally, it was found that the orientation and alignment of the octahedral NPs inside each superlattice is crucial for observing such polarization-dependent behavior.

We begin by using optical simulations to probe different types of resonances in the superlattices. Previous work done by our group has shown that both plasmonic modes and FP type photonic modes exist and interact in superlattices composed of spherical NPs (Figure 2A).[27] These two types of modes couple strongly to each other, leading to band gap behavior in some cases.[27,30] Here, FDTD simulations with an infinite slab model were used to approximate the optical properties of the superlattices. This model matches well with the experimental setup, which is described in detail in the Supporting Information (SI). Two polarizations, 0° and 90° (perpendicular and horizontal to the long axis of the rhombic dodecahedron, respectively), are used to characterize the light polarization (Figure 2A).

Importantly, the LSPRs of the octahedral NPs along 0° and 90° are different due to anisotropy of the NP shape (shape anisotropy, Figure 1). In addition, the top and bottom facets of the superlattice adopt the (110) plane of the bcc lattice structure,[31] resulting in a smaller interparticle spacing between NPs in 90° compared to 0°. The anisotropy in the lattice structure (structure anisotropy) would result in different interparticle interactions that depend on polarization, with sufficient volume fractions, even for superlattices composed of spherical NPs, where the NP shape anisotropy is absent. The solid lines in Figure 2B,C show the simulated backscattering spectra of superlattices made from spherical and octahedral NPs, respectively. The average diameter of the spherical NPs is 40 ± 3.2 nm, while the edge length of octahedral NPs is 51 ± 2 nm. Tips of the octahedral NPs are rounded with an average radius of curvature of 4.8 ± 0.5 nm, a value determined from scanning electron microscopy (SEM) images of the as-synthesized NPs used in the experiments (Figure S1). These NP structural parameters are kept constant throughout this work. The interparticle spacing, defined as the NP surface-to-surface distance along the 90° direction, is 40 nm, and the thickness of the slab is set to be 1.5 μm. These parameters are set such that they fall within a range that can be realized experimentally.[22,32−35]

The simulated spectra exhibit a convolution of plasmonic and FP modes, however, the influence of nano- and microscale structure can be disentangled (Figure 2). FP modes are purely

DOI: 10.1021/acs.nanolett.6b05101
Nano Lett. 2017, 17, 2313−2318

photonic modes that are determined by superlattice thickness and effective refractive index within the cavity. Therefore, we eliminate FP modes by simulating a 1 unit cell (u.c.) thick superlattice, where the superlattice is optically too thin to support any FP modes; such a structure should only exhibit the optical response of the plasmonic nanoparticles.[29] Indeed, only one peak is observed for the 1 u.c film (dashed lines, Figure 2B,C). Moreover, this peak is spectrally close to the main peak found in the thicker samples (1.5 μm). Therefore, the main peak in these figures is primarily determined by the plasmonic properties of a single layer of NPs, while the dips at longer wavelengths are from FP modes (orange arrows, Figure 2B,C).

From these simulations, we find that for the superlattices with spherical NPs there is negligible difference between the main peaks, namely the backscattering maximum around 560 nm, along the 0° and 90° polarizations. However, for the superlattices with octahedral NPs the main peak at around 610 nm red shifts by $\Delta\lambda \sim 10$ nm when the polarization is aligned along 90° compared to 0°. This difference suggests the crucial role that shape anisotropy plays. Notably, Maxwell-Garnett effective medium theory (EMT), which has been used to quantitatively explain a variety of optical properties in spherical nanoparticle based superlattices,[24,27,36,37] can no longer be applied to the superlattice made from octahedral NPs.

To experimentally demonstrate the different responses to the two polarizations in the two types of superlattices, spherical and octahedral NPs were assembled into bcc lattices with a rhombic dodecahedral crystal habit and ~2 μm parallel face-to-face dimensions (Figure 1, see SI for synthetic details). In particular, the directional DNA interaction will align octahedral NPs in a face-to-face manner,[20] as can be seen in the schematic drawing of a single unit cell superlattice in the (100) orientation (Figure S2A). After the assembly, the superlattices undergo a silica embedding process in order to preserve their structure in the solid-state,[38] enabling optical measurements and electron microscopy imaging. Small angle X-ray scattering (SAXS) was used to extract information on the crystal structure and lattice constant (in the solution- and in the solid-state), as well as to ensure their high quality crystallinity (Figure S2).

Backscattering measurements were performed on these superlattices with a microscope-coupled spectrometer (see SI for more information). Figure 3A,C shows SEM images of typical superlattices made from spherical and octahedral NPs, respectively, where the lattice constants, as measured by SAXS, are 69 and 102 nm, respectively. As such, the interparticle spacing is 29 nm for the spherical NPs and 37 nm for the octahedral NPs. The good agreement between simulation (top) and experiment (bottom) for both superlattices, Figure 3B,D, validates both the simulation model and the high quality and fidelity of the DNA-programmed NP superlattices. Polarization dependence is primarily observed for the main peak as dictated by nanoscale effects, such as NP shape, which controls the LSPR, and structure anisotropy of the lattice, which affects particle−particle coupling. At wavelengths far from the main peak, both simulation and experiment show a much smaller difference between the FP modes at the two polarizations.

To explore the effect of both shape and structure anisotropy, a set of superlattices where the interparticle spacing is varied from 20 to 70 nm and the superlattice thickness is held constant at 1.5 μm were simulated. Figure 4A summarizes the difference between the main peak along the 90° and 0° directions, namely, $\Delta\lambda = \lambda^{90}_{max} - \lambda^{0}_{max}$. A spectral representation can be seen in Figure 4B, where the backscattering spectra of

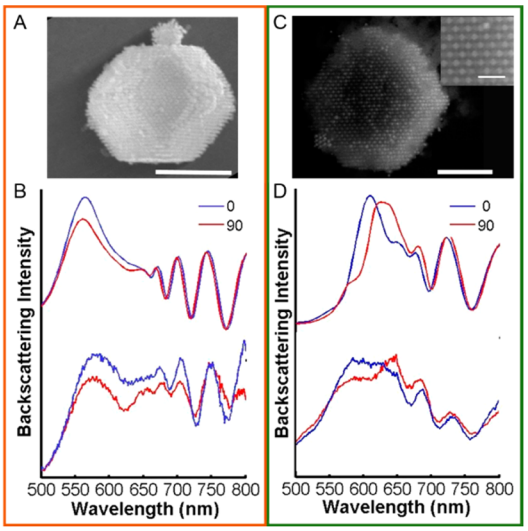

Figure 3. Experimental confirmation of the absence and presence of polarization-dependence in superlattices composed of spherical and octahedral NPs, respectively. (A,B) SEM image of a superlattice consisting of spherical NPs and its backscattering spectra obtained from simulation (top) and experiment (bottom). (C,D) The same set of data for a superlattice consisting of octahedral NPs. Inset in (C) is a magnified area of the SEM image. The interparticle spacings are 29 and 37 nm for superlattices made of spherical and octahedral NPs, respectively. Scale bars are 1 μm for (A,C), and 200 nm for inset in (C).

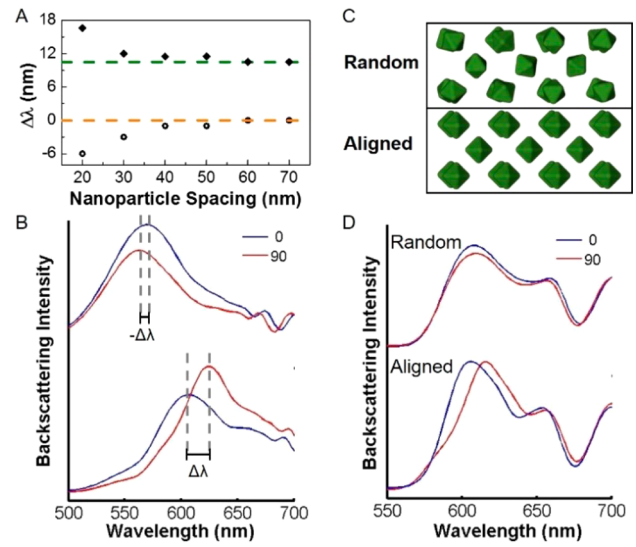

Figure 4. Effect of structural and NP shape anisotropy and NP alignment on polarization dependence. While keeping the NP size and shape the same, simulations show the effect of changing the interparticle spacing from 20 to 70 nm for spherical and aligned octahedral NPs. Differences between maxima of the main peaks at 90° and 0° polarization ($\Delta\lambda$) for all superlattices are summarized in (A). (B) Simulated spectra of spherical and aligned octahedral NPs with 20 nm interparticle spacing. Interestingly, for the superlattices consisting of spherical NPs, the peaks blue shift at 90° compared to 0°, resulting in negative $\Delta\lambda$ values as marked by the $-\Delta\lambda$. The opposite happens for the superlattices consisting of octahedral NPs. (C) In order to show the importance of alignment of the NPs, a set of simulations was set up with the same set of parameters but for randomly oriented (top) and well-aligned (bottom) NPs. Interparticle spacing here is 70 nm. (D) The backscattering spectra from the setup in (C). The polarization dependence is lost in the former case.

DOI: 10.1021/acs.nanolett.6b05101
Nano Lett. 2017, 17, 2313−2318

superlattices made from spherical (top) and octahedral (bottom) NPs with 20 nm interparticle spacing are plotted. In contrast with the polarization-dependent red shift as seen in the superlattices with octahedral NPs, the main peak blue shifts when the polarization is changed from 0° to 90° in the superlattices with spherical NPs, resulting in negative values of $\Delta\lambda$. In fact, as the interparticle spacing decreases, λ_{max} along both 0° and 90° are red-shifted, though the shift is more significant along 0° for superlattices made of spherical NPs (Figure S8). This red shift with decreasing NP separation is routinely observed and attributed to enhanced interparticle coupling.[8,39,40] However, the opposite trend (blue-shifting) is observed for the polarization dependence, by which we mean that although the NPs are more closely spaced (smaller interparticle spacing) along the 90° direction, λ^{90}_{max} is to the blue of λ^{0}_{max} for spherical NP superlattices.

Evidently, in this case long-range coupling between many NPs plays an important role, necessitating explicit consideration of the dipole lattice sum. Under the assumption that each NP can be considered as a point dipole, this sum describes the near- and far-field coupling between NPs and is solely dependent on the geometric parameters of the lattice (i.e., the arrangement of the NPs). Section V of the SI provides details of the lattice sum approach, here presented in the context of a coupled dipole method that uses the modified long-wavelength approximation to describe particle polarizabilities.[41,42] Applying this method to calculate the extinction spectra for a (110) bcc lattice plane along 0° and 90° (Figure S5) shows that the blue shift seen in superlattices made of spherical NPs is due to the difference in the lattice sums for the two polarization directions.[8,9,43] As the interparticle spacing increases (>60 nm), negligible polarization dependence is observed (Figure 4A), and the dipole lattice sums and extinction spectra (Figure S9) show that this is due to the smaller difference in the lattice sums along the different polarization directions for this spacing. Likewise, the larger red shifts of λ^{0}_{max} compared to λ^{90}_{max} as the interparticle spacing decreases can be attributed to a larger difference in the lattice sums along the two polarizations.

For superlattices made of octahedral NPs, λ^{90}_{max} is to the red of λ^{0}_{max}. Although the dipole lattice sum is the same for the same NP arrangement, compared to the case of superlattices made of spherical NPs, octahedral NPs have different effective polarizabilities (α) along the different polarization axes. Larger values of α along the 90° (tip-to-tip) will result in a reduced ($1/\alpha$), which would then intersect the dipole lattice sum at larger wavelength (Figure S5), which red shifts the resonance position (λ_{max}). In other words, a stronger tip-to-tip coupling along 90° contributes to a more significant red shift compared to edge-to-edge coupling along 0° as the interparticle spacing become small (Figure S12). As the interparticle spacing decreases, large plasmonic coupling plays an especially important role in the large red shift observed in λ^{90}_{max}.

As a result, the effect of structure anisotropy (i.e., different dipole lattice sums) on the polarization dependence becomes significant for both superlattices made of spherical and anisotropic NPs, respectively, at close distances (Figure 4A) with $\Delta\lambda$ becoming nonzero even for spherical NPs. The same trends are also demonstrated experimentally (see details in SI). From these data, we conclude that structural anisotropy is important only in close-packed superlattices (interparticle spacing <40 nm, see Figures S6−8),[7,37] while at larger interparticle spacings, the polarization dependence and lack thereof are determined by the NP shape anisotropy.

So far, the interparticle spacing of superlattices composed of octahedral NPs that can be realized by DNA-mediated assembly falls within a region where the effect of NP shape anisotropy dominates, namely larger interparticle spacing. It is likely that alignment of the NP building blocks is necessary in order to achieve polarization-dependent far-field properties. The effect of NP alignment can be easily probed by simulation where the local orientation of the NPs can be randomly varied while their location within the lattice and spacing remains fixed (Figure 4C). The results are then averaged over 10 randomized systems, similar to a model used previously to explore structural variation in spherical NP experiments, which provided strong agreement with experiment.[37] In order to prevent nearest neighbor NPs from touching each other in fully random orientations, a larger lattice constant, 135 nm, must be used, which corresponds to 70 nm interparticle spacing in the aligned superlattice. The results in Figure 4D illustrate that with larger interparticle spacing the polarization dependence is no longer observed for the randomized orientation superlattice. In other words, alignment of the NPs in the superlattice is necessary to generate a polarization-dependent plasmonic response, especially for larger interparticle spacing.

In conclusion, this work shows how one can uniquely use DNA-programmable assembly with electrodynamics simulations to interrogate specific structure−function relationships in well-defined microscopic crystals. The methodology allows one to focus on one set of parameters, isolated in large part from the others, including particle size and shape, lattice parameters, and crystal habit size. In this work, we have used it to identify a polarization dependence observed in lattices formed from spherical particles due to the bcc lattice symmetry, and a much stronger polarization dependence with lattices constructed from octahedral particles. The origin of this strong polarization dependence derives from both the shape of the octahedral particle building blocks as well as their arrangement into a well-defined lattice, where they are both positionally and rotationally ordered by virtue of DNA-programmed assembly. Moreover, the incorporation of anisotropic NPs introduces additional interesting features that were not accessible with spherical NP-based structures. Polarization-dependent properties associated with the superlattices derived from octahedral NPs open paths to polarization-dependent optical microdevices and electromagnetic field enhancement applications. As such, the robustness and tunability of DNA-programmable assembly coupled to the introduction of anisotropic NP building blocks further expands the platform of DNA-programmable assembly as a promising tool for a wide range of applications, spanning sensing, metamaterials, and micro-optical systems.

■ ASSOCIATED CONTENT

Supporting Information

The Supporting Information is available free of charge on the ACS Publications website at DOI: 10.1021/acs.nanolett.6b05101.

SEM and SAXS data of assembled superlattices. Summary of DNA design used in assembly. FDTD and coupled dipole calculations for superlattices consisting of spherical NPs. Backscattering spectra of superlattices, composed of spherical and octahedral NPs with varying lattice constants. Experimental and simulation results for a superlattice composed of octahedral NPs with longer DNA linkers used (PDF)

DOI: 10.1021/acs.nanolett.6b05101
Nano Lett. 2017, 17, 2313−2318

AUTHOR INFORMATION

Corresponding Authors

*E-mail: g-schatz@northwestern.edu.
*E-mail: chadnano@northwestern.edu.

ORCID

Michael B. Ross: 0000-0002-2511-0594
Chad A. Mirkin: 0000-0002-6634-7627

Author Contributions

L.S. and D.J.P. designed the optical experiments and simulation. H.L. and J.C.K. synthesized, functionalized, and assembled octahedral and spherical NPs, respectively. L.S. carried out optical experiments and simulation. L.S., H.L., D.J.P., and M.B.R. analyzed the data. M.R.B. and G.C.S. performed the coupled dipole calculations. L.S., M.B.R., J.C.K. and C.A.M. wrote the paper. G.C.S. and C.A.M. supervised the research.

Notes

The authors declare no competing financial interest.

ACKNOWLEDGMENTS

L.S. is grateful for the fruitful discussion with Nicolas Large. This material is based upon work supported by the Air Force Office of Scientific Research under Award FA9550-12-1-0280; the Asian Office of Aerospace Research and Development under Award FA2386-13-1-4124; and the Vannevar Bush Faculty Fellowship program sponsored by the Basic Research Office of the Assistant Secretary of Defense for Research and Engineering and funded by the Office of Naval Research through grant N00014-15-1-0043. Computational work was supported by the Center for Bio-Inspired Energy Science, an Energy Frontier Research Center funded by the U.S. Department of Energy, Office of Science, Basic Energy Sciences under Award No. DE-SC0000989. This work made use of the EPIC facility of Northwestern University's NU*ANCE* Center, which has received support from the MRSEC program (NSF DMR-1121262) at the Materials Research Center. L.S. acknowledges International Institute for Nanotechnology for the Ryan fellowship, H.L. is grateful to the scholarship from China Scholarship Council (CSC) under the Grant CSC No. 201306310060, and M.B.R and J.C.K. gratefully acknowledge support from the NDSEG fellowship program.

REFERENCES

(1) Schuller, J. A.; Barnard, E. S.; Cai, W.; Jun, Y. C.; White, J. S.; Brongersma, M. L. *Nat. Mater.* **2010**, *9* (3), 193−204.
(2) Odom, T. W.; Schatz, G. C. *Chem. Rev.* **2011**, *111* (6), 3667−3668.
(3) Maier, S. A. *Plasmonics: Fundamentals and Applications*, 1st ed.; Springer: New York, 2007.
(4) Tame, M. S.; McEnery, K. R.; Ozdemir, S. K.; Lee, J.; Maier, S. A.; Kim, M. S. *Nat. Phys.* **2013**, *9* (6), 329−340.
(5) Kauranen, M.; Zayats, A. V. *Nat. Photonics* **2012**, *6* (11), 737−748.
(6) Stockman, M. I. *Opt. Express* **2011**, *19* (22), 22029−22106.
(7) Zhao, L.; Kelly, K. L.; Schatz, G. C. *J. Phys. Chem. B* **2003**, *107* (30), 7343−7350.
(8) Ross, M. B.; Mirkin, C. A.; Schatz, G. C. *J. Phys. Chem. C* **2016**, *120* (2), 816−830.
(9) Haynes, C. L.; McFarland, A. D.; Zhao, L.; Van Duyne, R. P.; Schatz, G. C.; Gunnarsson, L.; Prikulis, J.; Kasemo, B.; Käll, M. *J. Phys. Chem. B* **2003**, *107* (30), 7337−7342.
(10) Tao, A. R.; Ceperley, D. P.; Sinsermsuksakul, P.; Neureuther, A. R.; Yang, P. *Nano Lett.* **2008**, *8* (11), 4033−4038.
(11) Maier, S. A.; Brongersma, M. L.; Kik, P. G.; Meltzer, S.; Requicha, A. A. G.; Atwater, H. A. *Adv. Mater.* **2001**, *13* (19), 1501−1505.
(12) Chang, A. S. P.; Kim, Y. S.; Chen, M.; Yang, Z.-P.; Bur, J. A.; Lin, S.-Y.; Ho, K.-M. *Opt. Express* **2007**, *15* (13), 8428−8437.
(13) Luk'yanchuk, B.; Zheludev, N. I.; Maier, S. A.; Halas, N. J.; Nordlander, P.; Giessen, H.; Chong, C. T. *Nat. Mater.* **2010**, *9* (9), 707−715.
(14) Shalaev, V. M.; Cai, W.; Chettiar, U. K.; Yuan, H.-K.; Sarychev, A. K.; Drachev, V. P.; Kildishev, A. V. *Opt. Lett.* **2005**, *30* (24), 3356−3358.
(15) Rozin, M. J.; Rosen, D. A.; Dill, T. J.; Tao, A. R. *Nat. Commun.* **2015**, *6*, 7325.
(16) Gwo, S.; Chen, H.-Y.; Lin, M.-H.; Sun, L.; Li, X. *Chem. Soc. Rev.* **2016**, *45* (20), 5672−5716.
(17) Tao, A.; Sinsermsuksakul, P.; Yang, P. *Nat. Nanotechnol.* **2007**, *2* (7), 435−440.
(18) Shevchenko, E. V.; Talapin, D. V.; Murray, C. B.; O'Brien, S. *J. Am. Chem. Soc.* **2006**, *128* (11), 3620−3637.
(19) Srivastava, S.; Nykypanchuk, D.; Fukuto, M.; Halverson, J. D.; Tkachenko, A. V.; Yager, K. G.; Gang, O. *J. Am. Chem. Soc.* **2014**, *136* (23), 8323−8332.
(20) Jones, M. R.; Macfarlane, R. J.; Lee, B.; Zhang, J.; Young, K. L.; Senesi, A. J.; Mirkin, C. A. *Nat. Mater.* **2010**, *9* (11), 913−917.
(21) Zhang, Y.; Lu, F.; Yager, K. G.; van der Lelie, D.; Gang, O. *Nat. Nanotechnol.* **2013**, *8* (11), 865−872.
(22) Macfarlane, R. J.; Lee, B.; Jones, M. R.; Harris, N.; Schatz, G. C.; Mirkin, C. A. *Science* **2011**, *334* (6053), 204−208.
(23) Zhang, C.; Macfarlane, R. J.; Young, K. L.; Choi, C. H. J.; Hao, L.; Auyeung, E.; Liu, G.; Zhou, X.; Mirkin, C. A. *Nat. Mater.* **2013**, *12* (8), 741−746.
(24) Ross, M. B.; Ku, J. C.; Lee, B.; Mirkin, C. A.; Schatz, G. C. *Adv. Mater.* **2016**, *28* (14), 2790−2794.
(25) Kim, Y.; Macfarlane, R. J.; Jones, M. R.; Mirkin, C. A. *Science* **2016**, *351* (6273), 579−582.
(26) Ku, J. C.; Ross, M. B.; Schatz, G. C.; Mirkin, C. A. *Adv. Mater.* **2015**, *27* (20), 3159−3163.
(27) Park, D. J.; Zhang, C.; Ku, J. C.; Zhou, Y.; Schatz, G. C.; Mirkin, C. A. *Proc. Natl. Acad. Sci. U. S. A.* **2015**, *112* (4), 977−981.
(28) Fowles, G. R. *Introduction to Modern Optics*, 2nd ed.; Holt, Rinehart, and Winston: New York, 1975.
(29) Ross, M. B.; Ku, J. C.; Vaccarezza, V. M.; Schatz, G. C.; Mirkin, C. A. *Nat. Nanotechnol.* **2015**, *10* (5), 453−458.
(30) Huang, C.-p.; Yin, X.-g.; Wang, Q.-j.; Huang, H.; Zhu, Y.-y. *Phys. Rev. Lett.* **2010**, *104* (1), 016402.
(31) Auyeung, E.; Li, T. I. N. G.; Senesi, A. J.; Schmucker, A. L.; Pals, B. C.; de la Cruz, M. O.; Mirkin, C. A. *Nature* **2013**, *505* (7481), 73−77.
(32) O'Brien, M. N.; Girard, M.; Lin, H.-X.; Millan, J. A.; Olvera de la Cruz, M.; Lee, B.; Mirkin, C. A. *Proc. Natl. Acad. Sci. U. S. A.* **2016**, *113* (38), 10485−10490.
(33) O'Brien, M. N.; Lin, H.-X.; Girard, M.; Olvera de la Cruz, M.; Mirkin, C. A. *J. Am. Chem. Soc.* **2016**, *138* (44), 14562−14565.
(34) Senesi, A. J.; Eichelsdoerfer, D. J.; Brown, K. A.; Lee, B.; Auyeung, E.; Choi, C. H. J.; Macfarlane, R. J.; Young, K. L.; Mirkin, C. A. *Adv. Mater.* **2014**, *26* (42), 7235−7240.
(35) Macfarlane, R. J.; Jones, M. R.; Senesi, A. J.; Young, K. L.; Lee, B.; Wu, J.; Mirkin, C. A. *Angew. Chem., Int. Ed.* **2010**, *49* (27), 4589−4592.
(36) Ross, M. B.; Blaber, M. G.; Schatz, G. C. *Nat. Commun.* **2014**, *5*, 4090.
(37) Ross, M. B.; Ku, J. C.; Blaber, M. G.; Mirkin, C. A.; Schatz, G. C. *Proc. Natl. Acad. Sci. U. S. A.* **2015**, *112* (33), 10292−10297.
(38) Auyeung, E.; Macfarlane, R. J.; Choi, C. H.; Cutler, J. I.; Mirkin, C. A. *Adv. Mater.* **2012**, *24*, 5181.
(39) Prodan, E.; Radloff, C.; Halas, N. J.; Nordlander, P. *Science* **2003**, *302* (5644), 419−422.
(40) Shuford, K. L.; Meyer, K. A.; Li, C.; Cho, S. O.; Whitten, W. B.; Shaw, R. W. *J. Phys. Chem. A* **2009**, *113* (16), 4009−4014.

DOI: 10.1021/acs.nanolett.6b05101
Nano Lett. 2017, 17, 2313−2318

(41) Gunnarsson, L.; Rindzevicius, T.; Prikulis, J.; Kasemo, B.; Käll, M.; Zou, S.; Schatz, G. C. *J. Phys. Chem. B* **2005**, *109* (3), 1079−1087.
(42) Auguié, B.; Barnes, W. L. *Phys. Rev. Lett.* **2008**, *101* (14), 143902.
(43) Kelly, K. L.; Coronado, E.; Zhao, L. L.; Schatz, G. C. *J. Phys. Chem. B* **2003**, *107* (3), 668−677.

DOI: 10.1021/acs.nanolett.6b05101
Nano Lett. 2017, 17, 2313−2318